Monte Carlo approach to calculate ionization dynamics of hot solid-density plasmas within particle-in-cell simulations

D. Wu,[1,2,*] X. T. He,[3] W. Yu,[1] and S. Fritzsche[2,4,†]

[1]*State Key Laboratory of High Field Laser Physics, Shanghai Institute of Optics and Fine Mechanics, 201800 Shanghai, China*

[2]*Helmholtz Institut Jena, D-07743 Jena, Germany*

[3]*Key Laboratory of HEDP of the Ministry of Education, Center for Applied Physics and Technology, Peking University, 100871 Beijing, China*

[4]*Theoretisch-Physikalisches Institut, Friedrich-Schiller-University Jena, D-07743 Jena, Germany*

(Received 16 June 2016; revised manuscript received 1 December 2016; published 16 February 2017)

A physical model based on a Monte Carlo approach is proposed to calculate the ionization dynamics of hot-solid-density plasmas within particle-in-cell (PIC) simulations, and where the impact (collision) ionization (CI), electron-ion recombination (RE), and ionization potential depression (IPD) by surrounding plasmas are taken into consideration self-consistently. When compared with other models, which are applied in the literature for plasmas near thermal equilibrium, the temporal relaxation of ionization dynamics can also be simulated by the proposed model. Besides, this model is general and can be applied for both single elements and alloys with quite different compositions. The proposed model is implemented into a PIC code, with (final) ionization equilibriums sustained by competitions between CI and its inverse process (i.e., RE). Comparisons between the full model and model without IPD or RE are performed. Our results indicate that for bulk aluminium at temperature of 1 to 1000 eV, (i) the averaged ionization degree increases by including IPD; while (ii) the averaged ionization degree is significantly over estimated when the RE is neglected. A direct comparison from the PIC code is made with the existing models for the dependence of averaged ionization degree on thermal equilibrium temperatures and shows good agreements with that generated from Saha-Boltzmann model and/or FLYCHK code.

DOI: 10.1103/PhysRevE.95.023208

I. INTRODUCTION

Detailed information of ionization distributions of solid-density plasmas is important to a number of high-energy-density physics studies, such as laser-driven heavy-ion accelerations [1] and intense laser-solid interactions [2]. In general, ionization dynamics determine the density of the involved plasmas, one of the most important parameters in plasmas physics research. Particularly, for laser driven heavy-ion accelerations, the accurate calculations of charge-to-mass ratio (q/m) of heavy ions will directly influence their acceleration efficiencies. In the intense laser-solid interaction regime, the generation of resistive magnetic fields will effectively guide the propagation of electrons beams. The reasonable predictions of the so-called resistive magnetic fields are, in fact, significantly determined by the underlying ionization calculations.

At present, two widely applied models that predict an average ionization degree of atoms are Thomas-Fermi model [3] and Saha [4] ionization model. Both of the models, however, assume that plasma conditions are near thermal equilibrium. For laser-produced plasmas and intense beam-solid interactions, where many of the involved physical processes take place at the subpicosecond or picosecond scales [2,5–11], the equilibrium assumption is no longer correct. To account for the temporal evolution of the plasma ionization, an impact (collision) ionization (CI) model based on electron-ion collisional cross sections has been explored [12–14], which allows us to calculate ionization values in a much more natural manner than equilibrium models. This model directly describes the interparticle interactions in the plasmas and, thus, accounts for the multiparticle nature of real plasmas. Although the CI model allows improvements in dealing with nonequilibrium plasmas, it is still not complete since it does not account for the inverse process, i.e., electron-ion recombinations (RE) [15–18]. Besides, the ionization potential depression (IPD) should be taken into account when dealing with dense plasmas [19–25]; however, it is also ignored in the considered models [12–14,26].

The main challenge to understanding the ionization of solid-density plasmas (matter) is to incorporate self-consistently the nonlinear behavior in such strongly coupled dynamical systems, i.e., the matter's response to the surrounding plasmas and plasmas' response to the matter through CI, RE, and IPD processes. To describe the ionization dynamics of solid-density plasmas more systematically, we here propose and analyze a Monte Carlo approach that can be configured and embedded into existing particle-in-cell (PIC) simulation codes. In this approach, we use a collection of macroparticles to describe a plasma or matter of finite ion density. Here, a macroparticle can be regarded as the ensemble of real particles, i.e., a group of particles with "same" mass, charge state, position, and momentum. The electrons are classified, moreover, into bound and free ones, where the former are regarded as part of ions or atoms, and the latter are isolated as the surrounding plasmas. Since we consider a collection of a large number of particles and a picosecond temporal evolution of the system, the fine structures, such as subshell configurations, excitations and their inverse processes, are ignored in the present model. Only the dominant physical processes are taken into account, such as CI and RE. Furthermore, the IDP by the surrounding plasmas should also be taken into consideration. This is because it will lower the bounding energy of ions or atoms, which will then, in turn, affect both CI and RE processes.

The paper is organized as follows. The physical model concerning CI, RE, and IPD are introduced in Sec. II. In Sec. III, the model is embedded into a PIC simulation code. Comparisons between the full model and model without IPD

*wudong@siom.ac.cn

†s.fritzsche@gsi.de

or RE are performed and analyzed. Dependence of averaged ionization degree on thermal equilibrium temperatures is obtained by the PIC code. Comparisons with results generated from Saha-Boltzmann model and/or FLYCHK code are made. Summary and discussion are given in Sec. IV.

II. PHYSICAL MODEL

When temperature of plasma is high with the kinetic energy of free electrons exceeding the ionization potential of ions or atoms, there exists a possibility that the ion or atom will lose a bound electron by the colliding with energetic free electrons. Simultaneously, free electrons and charged ions also have the tendency to recombine together. Different from isolated atom or ion, the screening of plasmas would dramatically influence the atomic structure of ions or atoms that embedded in, resulting in the lowering of their bounding energies. The above three processes, CI, RE, and IPD, are usually ignored in high-temperature and low-density plasmas. While when dealing with solid-density plasmas, these processes should be self-consistently taken into account. In this section, a CI model based on electron-ion collisional cross sections, a RE model based on three-body-recombination, and an IPD model based on the pioneering works of Stewart and Pyatt are explored and implemented into an existing PIC simulation code.

A. Impact ionization

Generally, a cross section of ionization can be derived by establishing an electron-ion (or atom) collisional pair and taking into account the energy of the incoming electron as well as the ionization state of the ion. The pioneering work was done by Lotz [27], with the formula of the total cross section as follows:

$$\sigma^{\rm ci} = \sum_{i=1}^{N} a_i q_i \frac{\ln(E/P_i)}{E P_i}\{1 - b_i \exp[-c_i(E/P_i - 1)]\}, \quad (1)$$

where E is the energy of impact electron, P_i is the binding energy of electron in the ith sub-shell, q_i is the number of equivalent electron in the ith subshell, and a_i, of unit $10^{-14}\,\mathrm{cm^2eV^2}$, b_i, and c_i are individual constants, which are determined by experiment measurements or theoretical predictions. Reference [27] also tabulates these constants of ionization cross sections, and this table is applied in our computations below. Furthermore, following Eq. (1), the ionization cross section among neighboring levels, such as, Al-II to Al-III, can be formulated as follows:

$$\sigma_i^{\rm ci} = a_i q_i \frac{\ln(E/P_i)}{E P_i}\{1 - b_i \exp[-c_i(E/P_i - 1)]\}, \quad (2)$$

with $E \geqslant P_i$, where P_i is the ionization potential from i to $i+1$ charge state, such as Al^{2+} to Al^{3+}. Let us note, however, the fine structure levels are ignored in Lotz's model, for which the ionization stage is treated as from the ground state to the next ground state. This assumption here is reasonable, as the fine structure levels are averaged out by the collection of large number of particles. Furthermore, the electron impact ionization cross section can also be calculated using the relativistic multiconfiguration flexible atomic code (FAC) [28].

The impact ionization rate of ion or atom is

$$\nu_i^{\rm ci} = \int_{P_i}^{\infty} v_e \sigma_i^{\rm ci}(E) f_e(E) dE, \quad (3)$$

where E, v_e, and f_e are energy, velocity, and density of surrounding electrons with energy between E and $E + dE$. In PIC simulations, the integral perform a summation over all electrons that reside within the same cell as the given ion of interest. The expression for ν_i in this form can be time-consuming as it requires a double loops over all ions and electrons in the cell. The idea presented in Ref. [13] takes advantage of the specific scaling of the ionization cross section and electron velocity with energy, i.e., $\ln(E)/E$ and $\sqrt{E}$, respectively, whose product is not sensitive to E and can be taken outside the integration. When replaced by their averaged values, the impact ionization rate takes the form

$$\nu_i^{\rm ci} = \sigma_i^{\rm ci}(\bar{E})\bar{v} n_e\ (\mathrm{s^{-1}}), \quad (4)$$

where $\bar{E}$, $\bar{v}$, and n_e are the averaged energy, velocity, and density of electrons in a cell. However, we have found that the above method tend to underestimate the ionization degree. When $\bar{E} < P_i$, ionization cannot take place at all, as those energetic electrons, which play an important role in impact ionization, are averaged out in the above method. To improve the above method and simultaneously overtake the time-consuming double loops, our idea is as follows: (i) a loop over electrons generates the average electron energy $\bar{E}$; (ii) preparing three arrays, $\bar{E}_m$, $\bar{n}_{em}$, and $\bar{v}_m$ containing the averaged energy, density, and velocity of electrons with their energies spanned by $\bar{E}_m$ and $\bar{E}_m + dE$ (the array step and maximal energy are assumed to be $0.25 \times \bar{E}$ and $5 \times \bar{E}$); (iii) a loop over electrons is performed again to fulfill the arrays; (iv) ionization rate for each ion in a cell is calculated by the following formula,

$$\nu_i^{\rm ci} = \sum_{m=0}^{20} \sigma_i^{\rm ci}(\bar{E}_m)\bar{v}_m\bar{n}_{em}\ (\mathrm{s^{-1}}). \quad (5)$$

The ionization probability of the ion of interest is $p_i^{\rm ci} = 1 - \exp(-\nu_i^{\rm ci}\delta t)$, where δt is the time step of PIC simulation. We increase the ionization degree by one unit for each ion and simultaneously put in an electron with the same position, velocity, and weight as its host ion, when condition $r > p_i^{\rm ci}$ is satisfied, where r is the computer-generated random number. To ensure that the energy remains conserved in the computations, we reduce local kinetic energy by distributing a momentum reduction to all local electrons, which is equivalent to the ionization energy.

B. Electron-ion recombination

Usually, the ionization balance of a plasma is determined by the competing processes of CI and RE, as well as various excitation and de-excitation processes. In particular, the recombination of electrons and ions takes place mainly by three different reaction modes, the dielectronic (D-RE), radiative (R-RE), and three-body recombinations (TB-RE), respectively [15]. As we have analyzed, in our model only ground state of ions and atoms are concerned, and the contributions of D-RE are averaged out. Note that, R-RE is

TABLE I. Ionization potential of aluminium atom and ions from NIST [29] as implemented in our model.

Al	1	2	3	4	5	6	7	8	9	10	11	12	13
eV	5.980	18.80	28.40	119.9	153.8	190.4	241.4	284.5	330.1	398.5	441.9	2085.	2300.

the inverse process of direct photoionization, while TB-RE is the inverse process of electron impact ionization. R-RE process is known to predominantly fill the low-lying Redberg states, while TB-RE is mainly responsible in rapidly bringing the high Rydberg states into equilibrium [15]. Thus, the contributions of recombinations in our cases mainly arise from the TB-RE process, with $e + e' + \mathrm{A}^Z \rightarrow \mathrm{A}^{ZM} + e''$, where $ZM = Z - 1$ with Z of the ion charge state. In the TB-RE, the excess energy released by the recombining electron is carried away by the outgoing electron e'', so that the TB-RE does not involve any emission of photons.

Expression of TB-RE rate formula has a strong dependence on the relying impact ionization formula. Let us consider the detailed balance equation of species with ionization charge state i and $i+1$,

$$\frac{\partial n_i}{\partial t} = \nu_{i+1}^{\mathrm{re}} n_{i+1} - \nu_i^{\mathrm{ci}} n_i, \tag{6}$$

where n_i is the density of ions, ν_{i+1}^{re} is the three-body recombination rate, and ν_i^{ci} is impact ionization rate. In order to relate these rate coefficients, one observes that at the recombination-ionization equilibrium, we have $\nu_{i+1}^{\mathrm{re}} n_{i+1} = \nu_i^{\mathrm{ci}} n_i$. As the ionization equilibrium can be well described by the Saha-Boltzmann equation [15],

$$\frac{n_e n_{i+1}}{n_i} = \frac{g_e g_{i+1}}{g_i} \left(\frac{2\pi m_e k_B T_e}{h^2} \right)^{3/2} \times \exp\left(-\frac{P_i}{k_B T_e} \right), \tag{7}$$

one can obtain

$$\nu_{i+1}^{\mathrm{re}} = \frac{g_i}{g_e g_{i+1}} (\lambda_e)^3 n_e \times \exp\left(\frac{P_i}{k_B T_e} \right) \times \nu_i^{\mathrm{ci}}, \tag{8}$$

where $\lambda_e = \sqrt{h^2/2\pi m_e k T_e}$ is the thermal electronic de Broglie wavelength, g_e and g_i are the statistical weights, and ν_i^{ci} is the ionization rate as shown in Eq. (5). In Eq. (8), T_e is temperature of plasmas, which is a quantity that can only be obtained at thermal equilibriums. In the PIC calculations, the quantity T_e is replaced with the averaged electron kinetic energy, which can be calculated at any time, regardless of thermal equilibriums.

According to Eq. (8), the recombination rate is increased dramatically in low-temperature and high-density plasma environment. Note that all the TB-RE formulas [16–18] exhibit this behavior, except for the slightly different numerical factors. In PIC simulations, the electron temperature T_e and electron density n_e can be generated by a loop over the electrons in each computational cell at every time step. Then Eq. (8) is applied for each ion resides in the same cell. The recombination probability is $p_i^{\mathrm{re}} = 1 - \exp(-\nu_i^{\mathrm{re}} \delta t)$, where δt is the simulation time step. We decrease ionization degree by one unit for each ion whenever the random number r satisfies $r > p_i^{\mathrm{re}}$. Again, to ensure that the energy remains conserved, the local kinetic energy, equivalent to the ionization energy, is increased, through a similar way as we have done in impact ionizations, by distributing a momentum modification to all local electrons. To ensure the conservation of remaining particles, the local plasma density, equivalent to recombinations, is reduced by distributing a weight modification to all local free electrons.

C. IPD by surrounding plasmas

The calculation of both impact ionization and electron-ion recombination requires values of ionization potentials, which, in principle, can be generated or obtained from data bases of National Institute of Standard and Technology (NIST). The ionization potential of aluminium atom (Al I) and ions are listed in Table I, which are calculated based on the isolated atom or ion model. However, in a plasma of finite density and temperature, the ionization potential of a given ion is influenced not only by its own bound electrons but also by the surrounding free electrons, which, in turn, will affect both impact ionization and recombination processes. Therefore, the phenomenon of ionization-potential depression for ions embedded in the plasma are of crucial importance for modeling atomic processes within dense plasmas. We here refer to the theory of IPD as introduced by Stewart and Pyatt [20], which is widely used in literatures of plasma and atomic physics calculations, including FLYCHK [30,31] code. The model yields ion-sphere and Debye-Huckel potential models as approximate limiting cases and could provide results over essentially the entire range of temperature and densities of plasmas. Let us here consider an ion (or atom), i, fixed in a sea of free electrons and ions at kinetic temperature T_e. The free electrons are described by relativistic Fermi-Dirac statistics and the ions by nonrelativistic Maxwell-Boltzmann statistics. For such a distribution of plasma electrons, the average electrostatic potential near i can be evaluated by Poisson equations. It is this potential that causes the IDP of the ion. The contributions of bound electrons to IPD are excluded, since they are already present in the isolated ion.

Following the work of Stewart and Pyatt [20], the lowering of ionization potential is described by

$$\Delta P = \frac{3(Z+1)e^2}{2R_i} \left\{ \left[1 + \left(\frac{\lambda_d}{R_i} \right)^3 \right]^{2/3} - \left(\frac{\lambda_d}{R_i} \right)^2 \right\}, \tag{9}$$

where λ_d is the Debye length $\lambda_d = \sqrt{T_e/4\pi Z n_e}$ with T_e of the free electrons (plasmas) temperature, and the ion-sphere radius is defined by $4\pi n_i R_i^3/3 = 1$, with n_i the ion number density. For large λ_d/R_i values, according to Eq. (9), ΔP is reduced to $(Z+1)e^2/\lambda_d$, which is the limit of Debye-Huckel model. When λ_d/R_i is small, ΔP equals to $3(Z+1)e^2/2R_i$, which is the limit of ion-sphere model. For high-density plasmas, the IDP would have a significant effect on lowing of ionization potential. For example, ΔP of Al VII (with the isolated ionization potential 240 eV) can be as large as 100 eV for bulk aluminium (2.7 g/cm^3) with temperature T_e below 300 eV. For going beyond such a semiempirical treatment, a rigorous way

of dealing with IDP is through multibody quantum-mechanical methods [21,22]. We have compared the values generated from Stewart and Pyatt's formula with that from references [21,22]. Results indicate that both calculation methods exhibit similar behavior, though with slightly different numerical values. In PIC simulations, ion density, electron density n_e, and temperature T_e can be generated by a loop over electrons in each computational cell, attached to which the Debye length λ_d is evaluated. Using Eq. (9) and isolated ionization potential value from NIST data bases, the modified ionization potential, i.e., $P - \Delta P$, is updated for each ion at every computational cell per time step.

III. APPLICATIONS

The above three processes are embedded in a recently extended version of PIC code based on LAPINE [32]. This is a parallel high-order-scheme PIC code written in C++ language, capable of performing 1D, 2D, and 3D simulations, with which the tunneling ionization [10], relativistic binary collisions [33], radiation reaction and photon emission in quantum electrodynamics regime [34] have already been implemented in by one of us. In this section, we will present several case studies of the ionization dynamics of bulk aluminium (single) and aluminium carbide (alloy). Let us note that the initially assumed charge state does not depend on the initial temperature in the following calculations, and that the free electron temperature is taken from a reasonable guess. The dependence of averaged ionization degrees on temperatures can only be established at (final) thermal equilibrium, after a reasonable relaxation time.

The density of bulk aluminium in our case studies is 2.7 g/cm^3, thus, the aluminium ion density is 6.6×10^{22}/cm^3. The initial aluminium charge state is assumed to be 4+, and the initial free-electron temperature is set to 150 eV. As a benchmark of the ionization dynamics, we consider only a few computational cells, connected by periodic boundaries conditions, with each cell contains 200 ion macroparticles and 200 electron macroparticles initially. The grid size of PIC simulation is 0.01 μm and time step is set to 0.02 fs. In the simulations, we have also taken into account the collision effects [33]. To figure out the influence of IPD and RE, three sets of simulations are run simultaneously. PIC simulations with full model (CI+IPD+RE), model without IPD, and model without RE are present in Figs. 1(a)–1(c), respectively. Figure 1(a) shows the total plasma energy (A.U.), with the full model by summarizing over all free electrons within a computational cell, as a function of time. Figures 1(b) and 1(c) are the same as shown in 1(a), but with the model excluding IPD and RE, respectively. Following the energy history, at initial time, the CI rate of aluminium is larger than RE. The former one would reduce the plasma energy and increase the averaged ionization degree as a function of time. Compared with Fig. 1(a), we found that after 6-ps relaxation, the averaged ionization degree is lowered when excluding the IPD, which is $\bar{Z} = 5.82$ with $T_e = 74$ eV (a) versus $\bar{Z} = 5.05$ with $T_e = 77$ eV (b). From the comparison of Figs. 1(a) and 1(c), we found that after 6-ps relaxation, the averaged ionization degree is significantly overestimated when excluding the RE process. Note that Fig. 1(c) also, in principle,

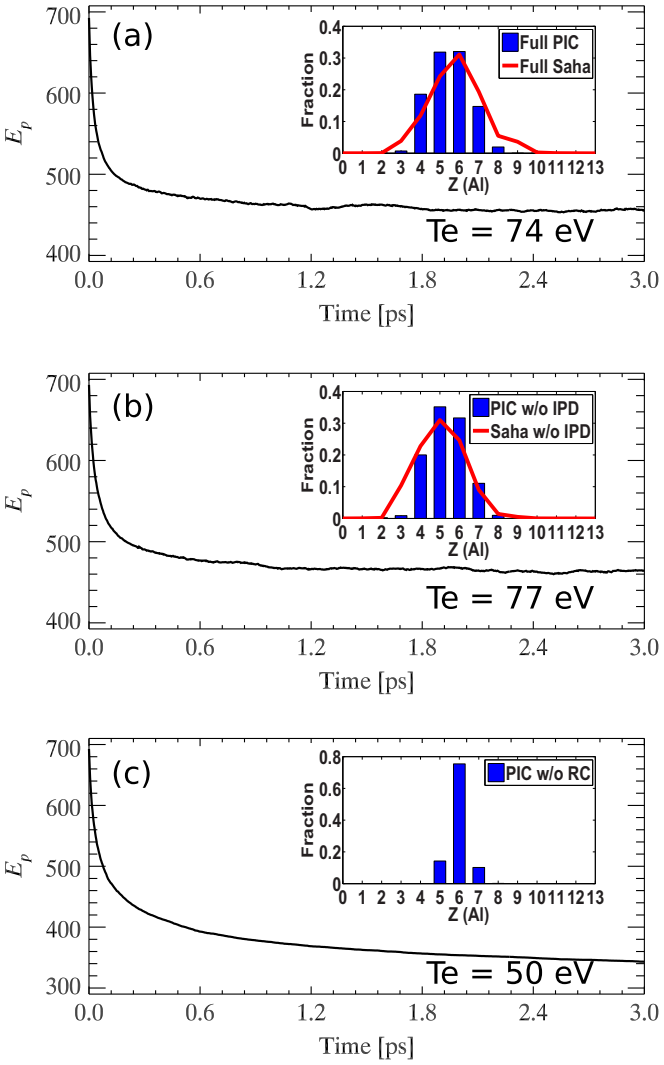

FIG. 1. (a) The total plasma energy (A.U.), with the full model by summarizing over all free electrons within a computational cell, as a function of time, with initial plasma temperature 150 eV and predefined charge state 4+. (b) The same as shown in panel (a), but with the model excluding IPD. (c) The same as shown in panel (a), but with the model excluding RE. The inlets over panels (a), (b), and (c) are the corresponding final ionization distributions of aluminium after 3-ps relaxation. The red line covered on the inlets are the ionization distributions of aluminium calculated by Saha-Boltzmann equation with defined temperature (a) $T_e = 74$ eV and (b) $T_e = 77$ eV also excluding IPD.

represent the results of existing PIC code [12–14,26], with which only CI is taken into account. As presented in Eq. (8), RE would become a dominant process for ions embedded in plasmas of high density and moderate temperatures.

Our model is general and can be applied for both single elements and alloys with quite different compositions. The aluminium carbide, chemical formula Al_4C_3, is a carbide of aluminium with density 2.36 g/cm^3. The simulation set is the same as shown in Fig. 1, but with an additional species carbon. Figure 2 shows the total plasma energy (A.U.), with the full model by summarizing over all free electrons within a computational cell, as a function of time, with the initial

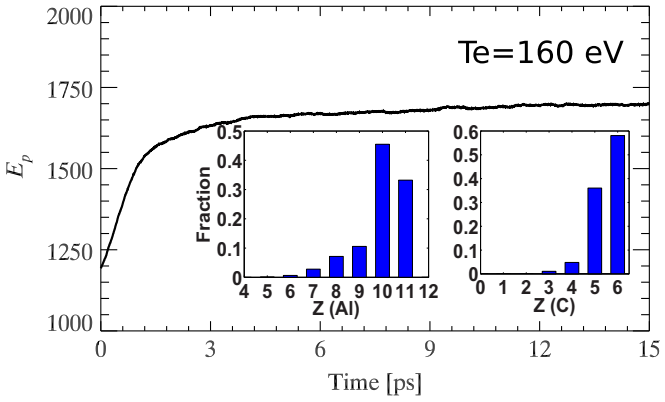

FIG. 2. The total plasma energy (A.U.), with the full model by summarizing over all free electrons within a computational cell, as a function of time, with the initial temperature of aluminium carbide 100 eV and predefined charge states of 11+ for aluminium and 6+ for carbon. The inlet is the final ionization distributions of aluminium and carbon after 15-ps relaxation.

temperature of aluminium carbide 100 eV and predefined charge states of 11+ for aluminium and 6+ for carbon. As shown in Fig. 2, thermal equilibrium is reached after 15-ps relaxation. The inlet is the final ionization distributions of aluminium and carbon with thermal equilibrium temperature 160 eV.

In our model, different strategies were used to ensure that the total number of particles remain conserved. The reduction of electrons due to recombination is through distributing a weight modification to all local free electrons, which does not change the number of macroparticles. While the increase of electron due to impact ionization is through placing *new* macroparticles to the cell of interest. The major computational effort in the simulation arises from the number of macroparticles. To solve this problem, a particle-merging technique is configured and applied. Considering two electrons with position $\boldsymbol{r}_a$ and $\boldsymbol{r}_b$, momentum $\boldsymbol{p}_a$ and $\boldsymbol{p}_b$, γ factors γ_a and γ_b, as well as weights w_a and w_b, we have the merging weight as $w = w_a + w_b$, merging position as $\boldsymbol{r} = (w_a\boldsymbol{r}_a + w_b\boldsymbol{r}_b)/w$, merging γ factor as $\boldsymbol{\gamma} = (w_a\gamma_a + w_b\gamma_b)/w$, and the merging momentum as $\boldsymbol{p} = (w_a\boldsymbol{p}_a + w_b\boldsymbol{p}_b)/w$. In practice, the equation, $\gamma = \sqrt{p^2 + 1}$, is not always satisfied for the *merged* particles. To solve this problem, a coefficient of $\eta = \sqrt{(\gamma^2 - 1)/p^2}$ is multiplied to replace the old merging momentum, with $\boldsymbol{p} = \eta\boldsymbol{p}$. The case shown in Fig. 1(a) is rerun by including the merging-particle technique. Figure 3(a) shows how the total plasma energy evolves in time, while Fig. 3(b) displays the corresponding number of macroparticles. Both the energy evolution and final equilibrium shown in Fig. 3(a) is exactly the same as shown in Fig. 1(a). In simulations, merging can be set to take place at predefined times when satisfying predefined conditions. In the case simulation shown in Fig. 3, merging is set to take place at every 100 time steps when number of macroparticles in a cell exceeding 1000 (200 macroparticles are placed in a cell initially). To make this technique numerical stable, we would suggest the threshold of merging to be set to $3 \sim 5$ times the initial number of macroparticles in a cell. As we can see, the dropping of the

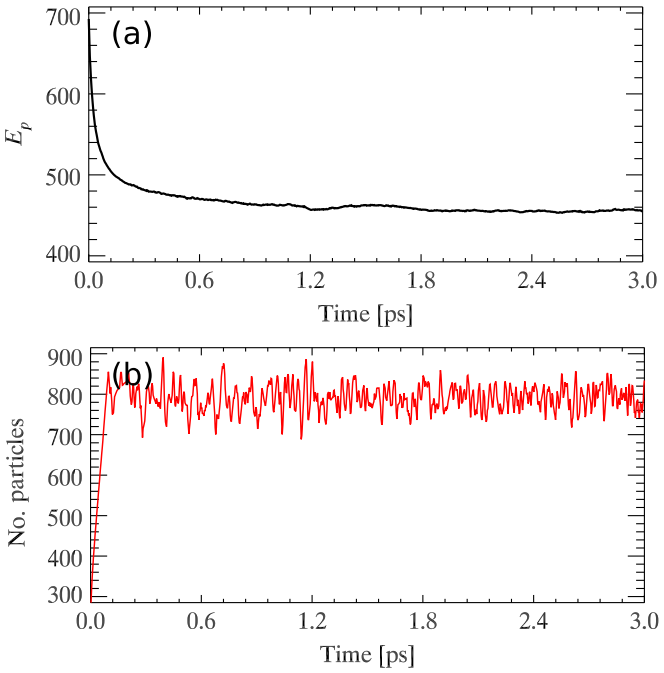

FIG. 3. (a) The total plasma energy (A.U.), with the full model and merging particle technique by summarizing over all free electrons within a computational cell, as a function of time, with initial plasma temperature 150 eV and predefined charge state 4+. (b) The corresponding temporal fluctuation of the number of macroparticles.

total number of macro particles does not affect the energy evolution or final equilibrium. By using this technique, the simulation burden can be dramatically released.

At present, we have compared with model calculation *with* and *without* the IPD and RE, a comparison that refers to the PIC code itself. In this section, a direct comparison with equilibrium models is made. As we have mentioned, the ionization equilibrium is described by the Saha-Boltzmann equation, with $n_e n_{i+1}/n_i = (g_e g_{i+1}/g_i)(2\pi m_e k_B T_e/h^2)^{3/2} \times \exp(-P_i/k_B T_e)$, where n_e (n_i), g_e (g_i), P_i, and T_e are electron (ion) density, statistical weights, ionization potential, and thermal equilibrium temperatures. Note that P_i can be obtained from the NIST database [29]. While in dense plasma regime, as we have analyzed, P_i should be corrected by taking into account IPD, which can be calculated by Stewart and Pyatt's formula. To solve the above Saha-Boltzmann equation, a natural way is to (i) normalize the above equation by n_e, $\widetilde{n}_i = n_i/n_e$, (ii) establish an iterative scheme, (iii) guess a initial values of $\widetilde{n}_1$, $\widetilde{n}_2$, $\widetilde{n}_3 \ldots$, and (iv) loop the iterative scheme until the required resolution is satisfied. Results of solving Saha-Boltzmann equation by this method are shown in Fig. 4(a). The solid lines show the averaged ionization of aluminium as functions of electron density and temperatures, whereas the black, red, and green lines represent the ones with electron densities fixed at 10^{20} cm^{-3}, 10^{22} cm^{-3}, and 10^{24} cm^{-3}, respectively. In Fig. 4(a), we also present results obtained from FLYCHK, with which the ionization calculation is also based on the Saha-Boltzmann equation. Both methods indicate that for fixed electron density at 10^{20} cm^{-3}, averaged ionization degree is close to zero in low-temperature limit, while it becomes 1+ or 3+ when electron density is fixed

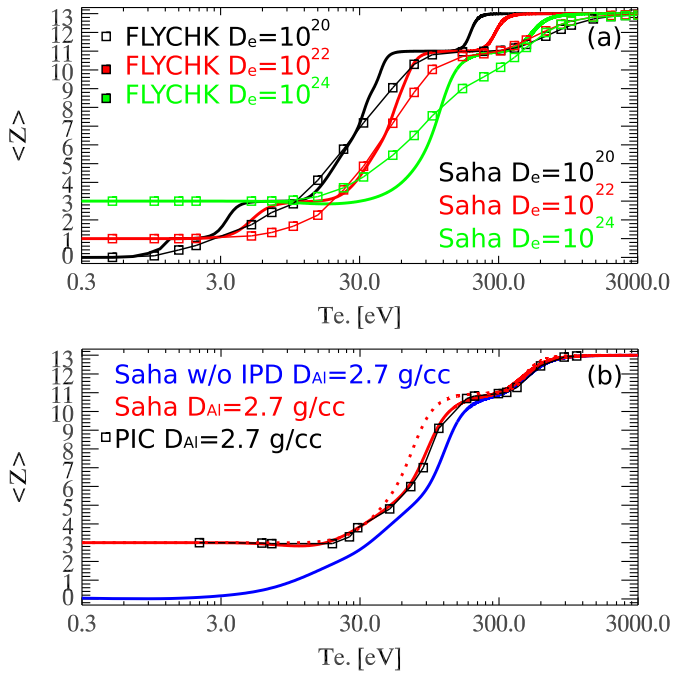

FIG. 4. The averaged ionization degree of bulk aluminium as a function of plasma temperature. (a) Blue, red, and green lines (square) are the results calculated by Saha-Boltzmann equation (FLYCHK code), with fixed electron density of 10^{20} cm^{-3}, 10^{22} cm^{-3}, and 10^{24} cm^{-3}. (b) Red and green lines are the results calculated by Saha-Boltzmann equation with updated numerical scheme, including IPD and excluding IPD, with fixed aluminium density 2.7 g/cm^3. Furthermore, solid red line is with the SP model of IPD, while dashed red line is with EK model of IPD. Black square is picked up from the equilibrium states calculated by our PIC code with full model.

at 10^{22} cm^{-3} or 10^{24} cm^{-3}. Actually, this nonzero averaged ionization degree is due to IPD. At high-density and low-temperature limit, the value of IPD can be even larger than the isolated ionization potential, which will free the $3p^1$ (and $3s^2$) electron.

It is hard for us to accurately predict the averaged ionization degree of a bulk aluminium without knowing both the plasma density and temperature in advance. This difficulty comes from the numerical scheme in solving the Saha-Boltzmann equation. In the first step of the numerical scheme, we normalize n_i by n_e. Although it is a quite natural way of doing so, in real situations, $n_{\rm Al}$ is fixed instead of n_e. Here we update the numerical scheme, with (i) normalizing n_i by $n_{\rm Al}$, $\widetilde{n}_i = n_i/n_{\rm Al}$ and (ii) adding a new constraint condition $\sum_{i=0}^{i=13} \widetilde{n}_i = 1$. For aluminium of fixed density $n_{\rm Al} = 6.7 \times 10^{22}$ cm^{-3}, the averaged ionization degree as a function of temperature is present in Fig. 4(b). Red and blue lines correspond to the cases including and excluding IPD. Results indicate that the averaged ionization degree when including IPD effect is indeed higher than excluding this effect. The averaged ionization degree is of $\bar{Z} = 3$ at low temperature limit. In addition, in Fig. 4(b) we also present the averaged ionization degree with Saha-Boltzmann equation and Ecker-Kroll (EK) model (refer to Appendix for detail). It is shown that in averaged ionization calculation, the difference between SP (solid red line) and EK (dashed red line) models is small.

In Figs. 1(a) and 1(b), the ionization distributions calculated by Saha-Boltzmann equation with updated numerical scheme is present in the red curves covered on the inlets, showing good consistence with the PIC calculations. Furthermore, following the same routine as introduced by Fig. 1, the dependence of averaged ionization degree on thermal equilibrium temperatures covering a large variation is obtained by the PIC code, as shown in black squares in Fig. 4(b), also showing good consistence with results from Saha-Boltzmann equation.

IV. CONCLUSIONS AND DISCUSSIONS

In summary, a physical model based on Monte Carlo approach is proposed to calculate the ionization dynamics of solid-density plasmas within PIC simulations, where CI, RE, and IPD by surrounding plasmas are taken into consideration self-consistently. When compared with other models, which are applied in the literature for plasmas near thermal equilibrium, the temporal relaxation of ionization dynamics can also be simulated by the proposed model. The proposed model is implemented into a PIC code, with (final) ionization equilibriums sustained by competitions between CI and RE. Comparisons between the full model and model without IPD or RE are performed. Results indicate that for bulk aluminium in the solid-density plasma regime, (i) the averaged ionization degree when including IPD effect would be higher than excluding this effect; and (ii) the averaged ionization degree is significantly overestimated when excluding RE effect. As a direct comparison with the existing models, dependence of averaged ionization degree on thermal equilibrium temperatures is obtained by the PIC code, showing good agreements with that generated from Saha-Boltzmann model and/or FLYCHK code.

The explicit RE formula is determined by the relying impact ionization formula and Saha-Boltzmann equation. The good agreements between values from PIC simulation at (final) thermal equilibrium and results from Saha-Boltzmann equation are thus guaranteed by the proposed model. However, let us note that the PIC code is a tool originally designed to describe high-temperature and low-density plasmas that are dominated by electromagnetic fields. The Fermi energy of aluminum, for example, is around 11 eV. Therefore, the methods and algorithms applied here only are suited to weakly coupled nondegenerate systems or "hot" plasmas with $T_e \gg 11$ eV. An accurate description of states of matters in which Fermi statistics and strong correlations dominate [35] is at present beyond the state-of-the-art PIC simulations.

ACKNOWLEDGMENTS

D. Wu acknowledges the financial support from German Academic Exchange Service (DAAD) and China Scholarship Council (CSC); thanks H. Xu at National University of Defence Technology; B. Goswami, J. W. Wang, and S. Z. Wu at Helmholtz Institut-Jena; and S. X. Luan at Shanghai Institute of Optics and Fine Mechanics for fruitful discussions.

APPENDIX: ECKER-KROLL MODEL

The Ecker-Kroll (EK) [19,21,24] model assumes two functional forms for the IPD, depending on whether the

particle density (i.e., that of both the electrons and ions) under investigation is above or below a critical density value, given by the expression $n_c = (3/4\pi)(T_e/Z_A^2 e^2)^3$, with $Z_A = 13$ for Al. For density below n_c, Debye-Huckel formula holds, i.e., $\Delta P = (Z+1)e^2/\lambda_d$, while for density above n_c, the EK model of the IPD is given by $\Delta P = C(Z+1)e^2/R_{EK}$, where $R_{EK}^3 = R_i^3/(Z+1)$ [refer to Eq. (9) for meaning of R_i] and C is a multiplication factor. The constant C is determined in the EK model by imposing that the IPD given by two functional forms equal with each other at the critical density, with $C = (R_{EK}/\lambda_d)_{n_c}$. The simulation of LCLS experiments, however, assumed $C = 1$ in the modified EK model [36].

[1] J. Braenzel, A. A. Andreev, K. Platonov, M. Klingsporn, L. Ehrentraut, W. Sandner, and M. Schnurer, Phys. Rev. Lett. **114**, 124801 (2015).

[2] P. Leblanc and Y. Sentoku, Phys. Rev. E **89**, 023109 (2014).

[3] D. Salzmann, *Atomic Physics in Hot Plasmas* (Oxford University Press, Oxford, 1998), pp. 27–28.

[4] I. H. Hutchinson, *Principles of Plasma Diagnostics* (Cambridge University Press, Cambridge, 1987).

[5] D. Wu, C. Y. Zheng, C. T. Zhou, X. Q. Yan, M. Y. Yu, and X. T. He, Phys. Plasmas **20**, 023102 (2013).

[6] D. Wu, C. Y. Zheng, B. Qiao, C. T. Zhou, X. Q. Yan, M. Y. Yu, and X. T. He, Phys. Rev. E **90**, 023101 (2014).

[7] M. Tabak, J. Hammer, M. E. Glinsky, W. L. Kruer, S. C. Wilks, J. Woodworth, E. M. Campbell, M. D. Perry, and R. J. Mason, Phys. Plasmas **1**, 1626 (1994).

[8] D. Wu, C. Y. Zheng, and X. T. He, Phys. Plasmas **20**, 063106 (2013).

[9] D. Wu, S. I. Krasheninnikov, S. X. Luan, and W. Yu, Nucl. Fusion **57**, 016007 (2017).

[10] D. Wu, B. Qiao, C. McGuffey, X. T. He, and F. N. Beg, Phys. Plasmas **21**, 123118 (2014).

[11] D. Wu, S. I. Krasheninnikov, S. X. Luan, and W. Yu, Phys. Plasmas **23**, 123116 (2016).

[12] Andreas J. Kemp, Robert E. W. Pfund, and Jurgen Meyer-ter-Vehn, Phys. Plasmas **11**, 5648 (2004).

[13] G. M. Petrov, J. Davis, and Tz. Petrova, Phys. Phys. Control. Fusion **51**, 095005 (2009).

[14] R. Mishra, P. Leblanc, Y. Sentoku, M. S. Wei, and F. N. Beg, Phys. Plasmas **20**, 072704 (2013).

[15] Yukap Hahn, Phys. Lett. A **231**, 82 (1997).

[16] Y. Hahn and J. Li, Z. Phy. D **36**, 85 (1996).

[17] P. Mansbach and J. Keck, Phys. Rev. **181**, 275 (1969).

[18] B. Makin and J. C. Keck, Phys. Rev. Lett. **11**, 281 (1963).

[19] G. Ecker and W. Kroll, The Phys. Fluids **6**, 62 (1963).

[20] John C. Stewart and Kedar D. Pyatt, JR Astr. Phys. J. **144**, 1203 (1966).

[21] M. Stransky, Phys. Plasmas **23**, 012708 (2016).

[22] Carlos A. Iglesias, High Energy Density Phys. **12**, 5 (2014).

[23] Sang-Kil Son, Robert Thiele, Zoltan Jurek, Beata Ziaja, and Robin Santra, Phys. Rev. X **4**, 031004 (2014).

[24] Carlos A. Iglesias and Philip A. Sterne, High Energy Density Phys. **9**, 103 (2013).

[25] Thomas R. Preston, Sam M. Vinko, Orlando Ciricosta, Hyun-Kyung Chung, Richard W. Lee, and Justin S. Wark, High Energy Density Phys. **9**, 258 (2013).

[26] F. Perez, L. Gremillet, A. Decoster, M. Drouin, and E. Lefebvre, Phys. Plasmas **19**, 083104 (2012).

[27] Wolfgang Lotz, Z. Physik **232**, 101 (1970).

[28] M. F. Gu, Astr. Phys. J. **582**, 1241 (2003).

[29] Refer to http://physics.nist.gov/PhysRefData/ASD/ for ionization energy data.

[30] H. K. Chung, M. H. Chen, W. L. Morgan, Y. Ralchenko, and R. W. Lee, High Energy Density Physics **1**, 3 (2005).

[31] Refer to https://www-amdis.iaea.org/FLYCHK/ for online computing.

[32] H. Xu, W. W. Chang, H. B. Zhuo, L. H. Cao, and Z. W. Yue, Chin. J. Comput. Phys. **19**, 305 (2002).

[33] D. Wu, X. T. He, W. Yu, and S. Fritzsche, Phys. Rev. E **95**, 023207 (2017).

[34] D. Wu, B. Qiao, and X. T. He, Phys. Plasmas **22**, 093108 (2015).

[35] Vojtech Vlcek, Nico de Koker, and Gerd Steinle-Neumann, Phys. Rev. B **85**, 184201 (2012).

[36] S. M. Vinko, O. Ciricosta, B. I. Cho, K. Engelhorn, H.-K. Chung, C. R. D. Brown, T. Burian, J. Chalupsky, R. W. Falcone, C. Graves, V. Hajkova, A. Higginbotham, L. Juha, J. Krzywinski, H. J. Lee, M. Messerschmidt, C. D. Murphy, Y. Ping, A. Scherz, W. Schlotter, S. Toleikis, J. J. Turner, L. Vysin, T. Wang, B. Wu, U. Zastrau, D. Zhu, R. W. Lee, P. A. Heimann, B. Naglerand J. S. Wark, Nature **482**, 59 (2012).